Electronic Supplementary Material (ESI) for Journal of Materials Chemistry A.

Supporting Information

Designed Sulfonate-Based Covalent Organic Frameworks with Dual Functions of Recognition and Encapsulation

Shuaishuai Shang, [a‡] Shuhao An, [a‡] He Li, [a] Jianping Li,[b] Shenping Zhang,[c] Changjun Peng,[a] Honglai Liu,[a] Jun Hu[a*]

[a] School of Chemistry and Molecular Engineering, East China University of Science and Technology, Shanghai 200237, P. R. China

[b] National Engineering Laboratory for Industrial Wastewater Treatment, East China University of Science and Technology, Shanghai 200237, P. R. China

[c] Shanghai Institute of Quality Inspection and Technical Research, Shanghai 200233, P. R. China

[*]Correspondence: junhu@ecust.edu.cn

[‡]These authors contribute equally to this work.

Methods

Fourier transform infrared spectroscopy (FT-IR) spectra were obtained with a Bio-Rad FTS-3500 ARX FT-IR spectrometer. Solid-state nuclear magnetic resonance (NMR) data were collected on a Bruker Avance 400 MHz NMR spectrometer (DRX400) with cross-polarization magic-angle-spinning (CP/MAS). Dynamic light scattering (DLS) tests were performed at room temperature using a Zetasizer (Nano Series, Malvern Instruments, UK). Scanning electron microscopy (SEM) were conducted on a Helios G4 UC SEM-FIB (15 kV) equipped with an energy dispersive spectrometer. Samples were treated via Pt sputtering before observation. The Brunauer−Emmett−Teller (BET) surface areas were calculated from N_2 sorption isotherms at 77 K using a Micromeritics ASAP 2020 surface area and pore size analyzer. Transmission electron microscopy (TEM) were conducted on a Talos F200X TEM. Atomic force microscopy (AFM) were observed on a Nano ManVS. Powder X-ray diffraction (PXRD) patterns were obtained on a Bruker D8 Advance X-ray powder diffractometer equipped with a Cu sealed tube (λ = 1.54178 Å) at a scan rate of 0.02° s^{-1}. Thermogravimetric analyses (TGA) were performed using a Shimadzu DTG-60AH in the temperature range of 25 to 800 °C under flowing N_2 (30 mL min^{-1}) with a heating rate of 10 °C min^{-1}. Fluorescence spectra were recorded on an F-4600 FL spectrophotometer equipped with a xenon lamp and quartz carrier at room temperature. UV−vis spectra were obtained with a UV-2600 spectrophotometer in the range of 250−800 nm at room temperature.

Materials and experimental procedures

Solvents, reagents and chemicals were commercially available and used without further purification. Triformylphloroglucinol (Tp) were prepared by previous reports.[1]

Synthesis of Tp. Tp was prepared according to previous reported literature procedure. Hexamethylenetetramine (15.098 g, 108 mmol) and dried phloroglucinol (6.014 g, 49 mmol) under N2 was added into 90 mL trifluoroacetic acid. The solution was heated and stirred at 100 ºC for ca. 2.5 h. Approximately 150 mL of 3 M HCl was added and the solution was heated at 100 ºC for 1 h. After cooling to room temperature, the solution was filtered through Celite, extracted with ca. 350 mL dichloromethane, dried over magnesium sulfate, and filtered. Rotary evaporation of the solution afforded an off-white powder, a pure sample was obtained by sublimation. 1H NMR (400 MHz, DMSO-d6, δ): 10.67 (s, 3H); 10.02 (s, 3H).

Synthesis of sulfonate-COF. In a typical procedure for the sulfonate-COF [2], a Pyrex tube measuring o.d.× i.d. =10 × 8 mm^2 was charged with 1,3,5-triformylphloroglucinol (TP, 21 mg, 0.1 mmol) and 2,5-diaminobenzene-1,4-disulfonic acid (DABDA, 40 mg, 0.15 mmol) in a solution of 0.75 mL of Mei / 0.75 mL of Dio / 0.2 mL of 6 M aqueous acetic acid. This mixture was sonicated for 10 min to form a homogeneous suspension. The tube was subsequently flash frozen at liquid N_2 temperature (77 K), degassed by three freeze−pump−thaw cycles, and then flame sealed. Finally, the reaction mixture was heated at 120 °C for 3 days under a static condition. After cooling, the brown precipitate was collected by filtration and washed with copious amounts of anhydrous THF, DMF, H_2O and MeOH. The raw product was further carefully purified via solvent exchange with anhydrous THF and acetone four times, thus achieving the residual guest and oligomer removal. The material was dried under vacuum at 80 °C overnight to afford sulfonate-COF as a brown powder with the yields of 78%.

Synthesis of TpPa-COF. The TpPa-COF without sulfonic acid groups were obtained from the similar synthetic procedures by changing the 2,5-diaminobenzene-1,4-disulfonic acid to p-phenylenediamine with the yields of 83%. The synthetic procedure and characterization were shown in Figure S4 and S5.

Synthesis of f-sCON. Due to the effect of sulfonic acid groups, bulk sulfonate-COF can be spontaneously exfoliated into nanosheets in aqueous solution. In the exfoliation experiment, sulfonate-based fluorescent CON was successfully prepared by putting 10 mg of sulfonated-COF powder into 100 ml deionized water, and then sonicated the mixed solution for 10 minutes to obtain a f-sCON aqueous solution. Once finished, the residual bulk sulfonate-COF was removed from the solution by filtration, and the aqueous solution was used for subsequent characterization and experiments.

Synthesis of gel. A solution of polyvinyl alcohol (PVA) was prepared by placing 5 g of PVA glue and 10 ml distilled water in beaker with mechanical stirrer. Here, a certain amount of glycerin was added to increase its water retention. Separately, 1 g of borax was slowly added with stirring vigorously, until a transparent gel was obtained.

Synthesis of f-sCON-gel. The f-sCON-gel was prepared by introducing f-sCON in the preparation process. The solution of PVA was prepared by placing 5 g of PVA glue to 10 ml above f-sCON aqueous solution. The subsequent operation was the same as the above synthesis of gel process. Finally, the sulfonate-based fluorescent CON gel (f-sCON-gel) was easily obtained.

Detection of antibiotics. In the fluorescent detection experiment of f-sCON, we took 2ml of the transparent aqueous solution containing f-sCON and placed it in a cuvette for fluorescence measurement. We prepared 0.5 x 10^{-3} M antibiotic solution and added it to the cuvette. Then the emission spectra were measured for data analysis from 330 to 600 nm at the excitation wavelength of 315 nm. All detection experiments were carried out in parallel three times to get a concordant value.

Limit of detection (LOD) calculation. The LOD detection method is similar to the literature.[3] According to the standard deviation (S_b) of fluorescence intensity detected in water for 20 times and the k_{sv} value calculated by Stern-Volmer (SV) equation, the LOD value was calculated.

$$S_b = \sqrt{\frac{\sum\left(1 - \frac{I_0}{I_1}\right)^2}{N-1}} \ (N = 20)$$

$$LOD = \frac{3S_b}{k_{sv}}$$

S_b is the standard deviation for replicating detections of blank f-sCON solutions; I_0 is the fluorescence intensity of f-sCON in water; I_1 is the average of the I_0.

Static adsorption Experiments. The adsorption isotherms of antibiotics were obtained by mixing 2.5 mg sulfonate-COF with 5 mL antibiotics solution of different concentrations at a constant temperature of 298 K. The amount of antibiotics adsorbed on the sulfonate-COF was calculated using the mass balance with equation:

$$q_e = \frac{(c_0 - c_e) \times v}{m}$$

Where q_e (mg g^{-1}) is the equilibrium adsorbed amount; c_0 and c_e (mg L^{-1}) are the initial and equilibrium concentrations of solution; v (mL) is the volume of solution; and m (mg) is the mass of sulfonate-COF. In order to ensure the accuracy of measurements, all the experiments were repeated at least three times, and the average values were reported.

The equilibrium adsorption isotherm data were fitted by using the Langmuir and Freundlich models. The Langmuir isotherm model equation can be defined by

$$\frac{c_e}{q_e} = \frac{1}{K_L q_m} + \frac{c_e}{q_m}$$

and the Freundlich isotherm model can be defined by

$$\ln q_e = \ln K_F + \frac{1}{n} \ln c_e$$

where q_e (mg g^{-1}) refers to the equilibrium adsorption capacity, c_e (mg L^{-1}) refers to the antibiotics concentration at equilibrium, q_m (mg L^{-1}) refers to the maximum adsorption capacity, K_L is the Langmuir constant, and K_F and n are the Freundlich constant and adsorption intensity, respectively.

For the exploration of the kinetic adsorption experiment, 50 mg sulfonate-COF adsorbent was added to 100 mL of 50 mg L^{-1} antibiotics solution. We took 5ml solution after different time of adsorption, then the following operations were the same.

The adsorption kinetic data were fitted with the pseudo-second-order model and the pseudo-first-order model, and the pseudo-second-order model can be represented as follows:

$$\frac{t}{q_t} = \frac{1}{k_2 q_e^2} + \frac{t}{q_e}$$

where q_e and q_t (mg g^{-1}) refer to the uptake capacity at equilibrium and given time t(min), respectively. k_2 (g mg^{-1} min^{-1}) refers to the pseudo-second-order rate constant of antibiotics adsorption. Plotting t/q_t against t can be used to obtain the slope and intercept corresponding to the k_2 and q_e.

The pseudo-first-order model can be represented as follows:

$$\ln\frac{q_e}{q_t} = -k_1 t$$

k_1 (min^{-1}) refers to the pseudo-first-order rate constant of antibiotics adsorption.

The recycling usage of adsorbents were conducted similar as the batch adsorption experiments. In each cycle, after TCH adsorption, the sulfonate-COF was regenerated by washing with water and ethanol for three times to remove TCH. Then, the regenerated sulfonate-COF was filtrated, dried at 80 ℃ for 6 h, and weighted again before the next cycle adsorption test.

Dynamic Adsorption Experiments. The dynamic adsorption experiments were performed based on a fixed-bed column system to investigate the continuous TCH removal efficiency. A total of 20 mg sulfonate-COF of studied adsorbents was thoroughly milled to pack the column and then rinsed and equilibrated with deionized water for at least 10 min before each experiment. A 50 mg L^{-1} TCH feed aqueous solution was continuously passed through the column bed with an elution rate of 10 mL min^{-1}. The filtrates at the column outlet were collected, and the corresponding TCH concentration was characterized by UV−vis spectrophotometer at regular intervals of 3 mL solutions.

Theoretical Calculations. We applied quantum calculation (QM) to investigate the binding energies of the guest molecules (antibiotics and solvents) with the sulfonate-COF segments:

$$E = E_{total} - E_{segment} - E_{guest}$$

Where the E is the binding energy between the COF and the guest molecules. $E_{segment}$, E_{guest}, and E_{total}, are the energies of the COF, guest molecules and their complex, respectively. All of the structures are optimized before energy calculation. Here, we used density functional theory (DFT) to calculate $E_{segment}$, E_{guest}, and E_{total}, which is performed by the Dmol3 module. The Perdew-Burke-Ernzerhof (PBE) method was used to approximate the exchange correlation energy. The double-numeric basis plus polarization orbitals (DNP) was used for valence electrons. The self-consistent framework (SCF) was used to solve the Kohn-Sham equations. The SCF iteration was assumed to converge when the energy change lower than 2.57×10^{-3} kJ mol^{-1}. The geometry optimization was assumed to converge when the energy change lower than 2.7×10^{-4} eV, force lower than 0.05 eV $Å^{-1}$, and displacement lower than 0.005 Å. The dispersion interaction via the D2 method of Grimme (DFT-D) is include in the calculations.

Molecular dynamics simulation. Simulated polymerization algorithm was performed through Dendrimer and Amorphous Cell package in Materials Studio to generate initial structure of sulfonate-COF with the density of 0.3 cm^3 g^{-1}. The COF cell were contained 200 H_2O molecules to prevent the stacking of the polymer chain and simulated as the water environment. The models were then subjected to NPT-MD runs to obtain the dynamic properties of COF nanosheets in water environment (T = 300 K, P = 1 bar, t = 2ns). The atom-atom interaction was modelled by the COMPASSII force field and the charges was set as Use Current. The electrostatic interaction was calculated by the Ewald summation method with an accuracy 1 x 10^{-5} kcal/mol. The long ranges tail of the Lennard–Jones (LJ) potential is truncated at 12.5 Å, where the discontinuity of the interacting potential at the truncation point is smoothed by the cubic spline method with a spline width 1 Å and a buffer width 0.5 Å.

Supporting Figures

Figure S1. FT-IR spectra of TP (black); DABDA(red) and sulfonate-COF (blue).

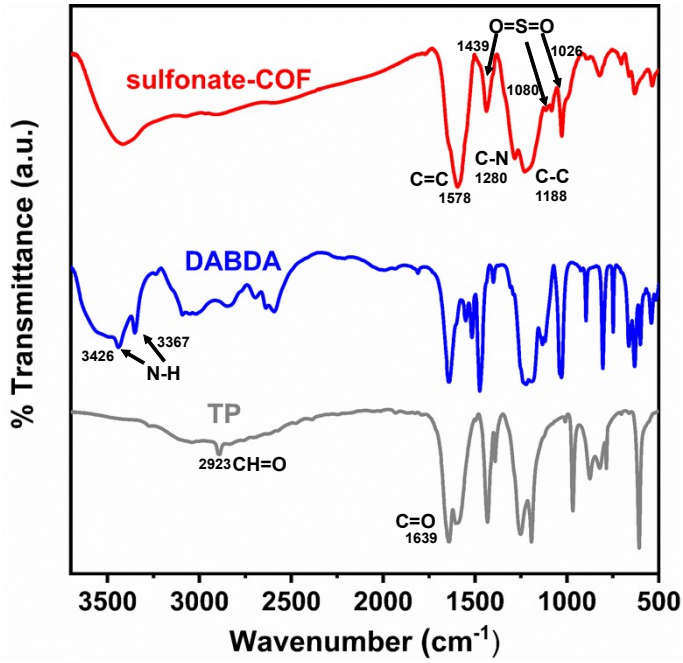

Figure S2. ^{13}C SSNMR spectrum of sulfonate-COF.

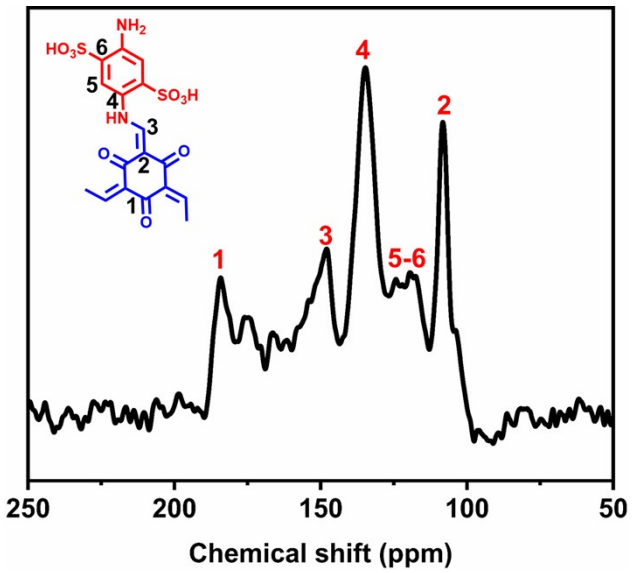

Figure S3. (a) Nitrogen adsorption isotherm of sulfonate-COF measured at 77 K; (b) Pore size distribution profiles of sulfonate-COF based on NLDFT.

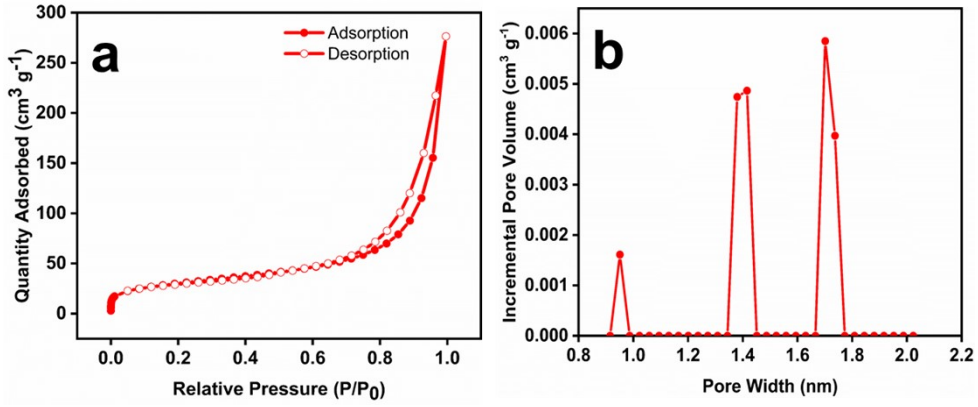

Figure S4. Synthesis and structure of TpPa-COF.

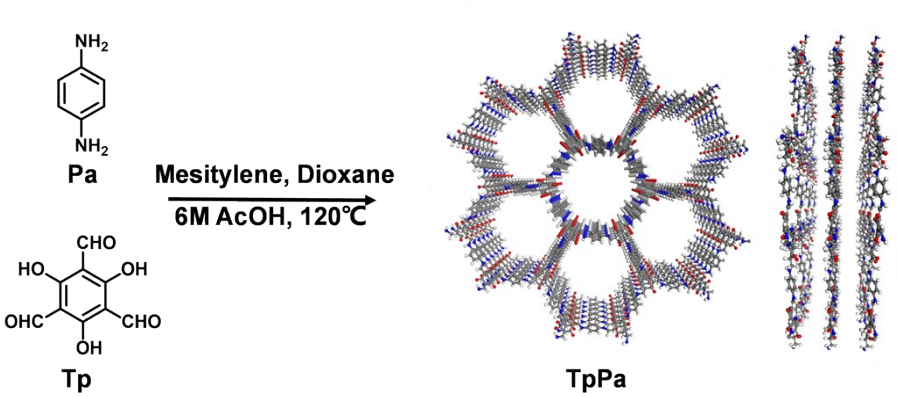

Figure S5. (a) PXRD profiles of TpPa-COF (black curves) and simulated for AA stacking (red curves); (b) Nitrogen adsorption isotherm of TpPa-COF measured at 77 K.

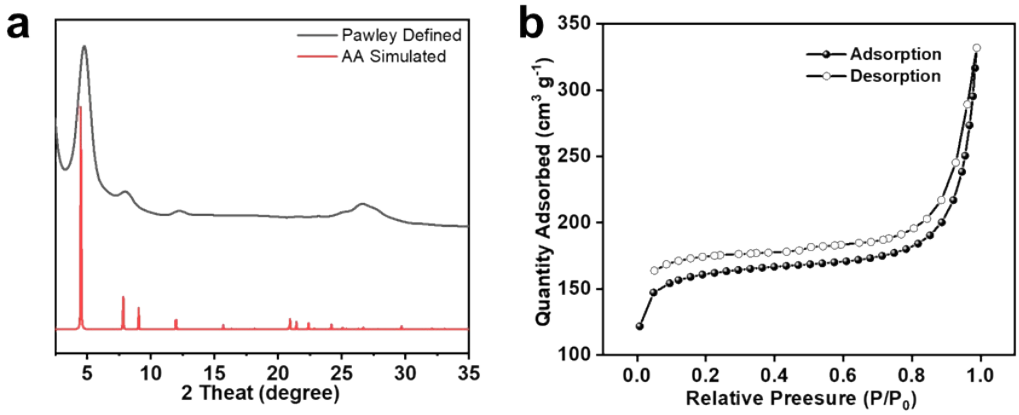

Figure S6. TGA curve of sulfonate-COF (red), TpPa-COF (black)

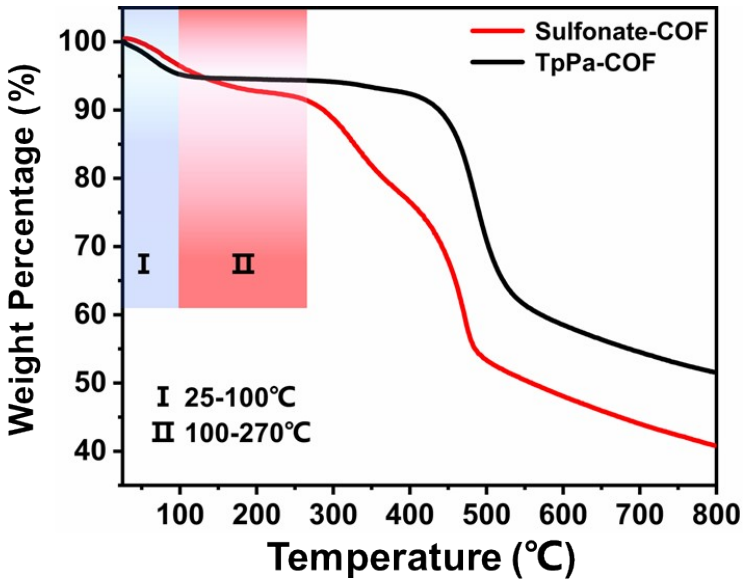

Figure S7. The FTIR of pristine sulfonate-COF (black) and H_2O-adsorbed sulfonate-COF (red).

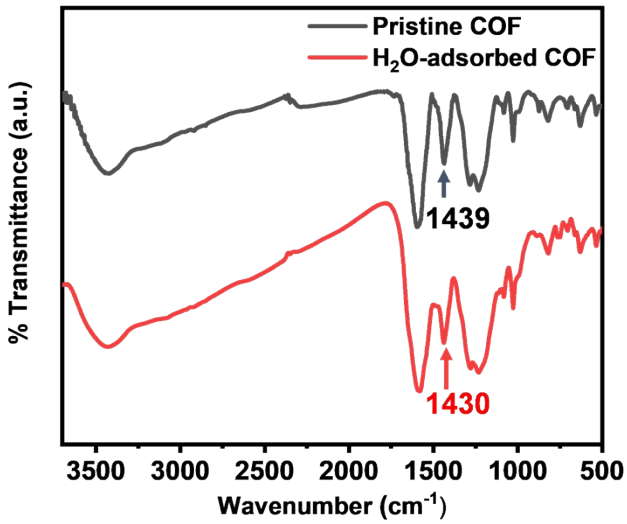

Figure S8. 11 snapshot images of the MD simulation procedure focusing on sulfonate-COF in aqueous medium demonstrating self-exfoliation (White: H; Blue: N; Gray: C;Yellow: S;Red: O).

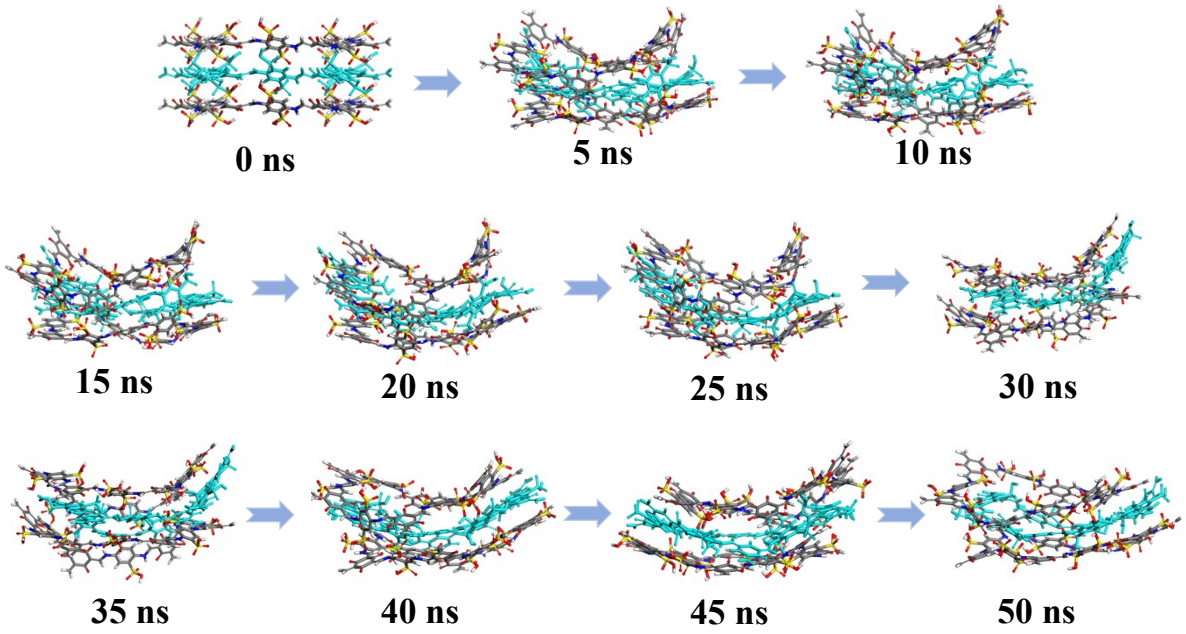

Figure S9. MSD of sulfonate-COF relative to its original position in the crystal structure over the 50 ns simulation.

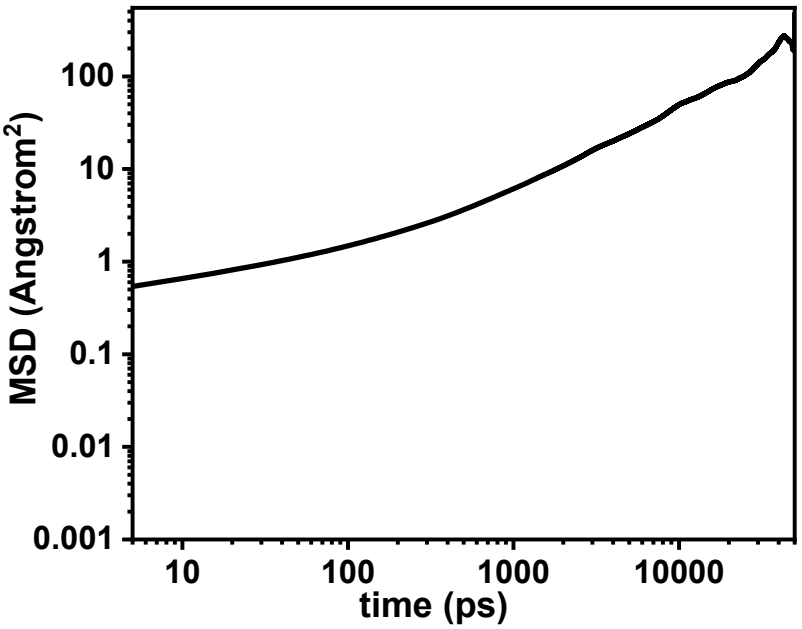

Figure S10. 11 snapshot images of the MD simulation procedure focusing on TpPa-COF in aqueous medium demonstrating self-exfoliation (White: H; Blue: N; Gray: C; Red: O).

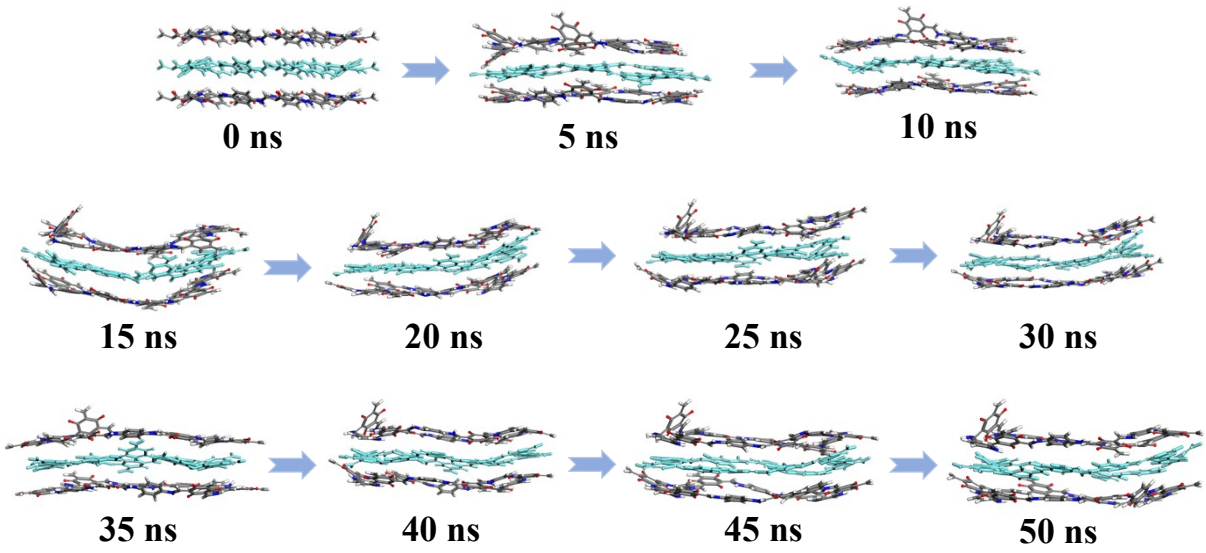

Figure S11. MSD of TpPa-COF relative to its original position in the crystal structure over the 50 ns simulation.

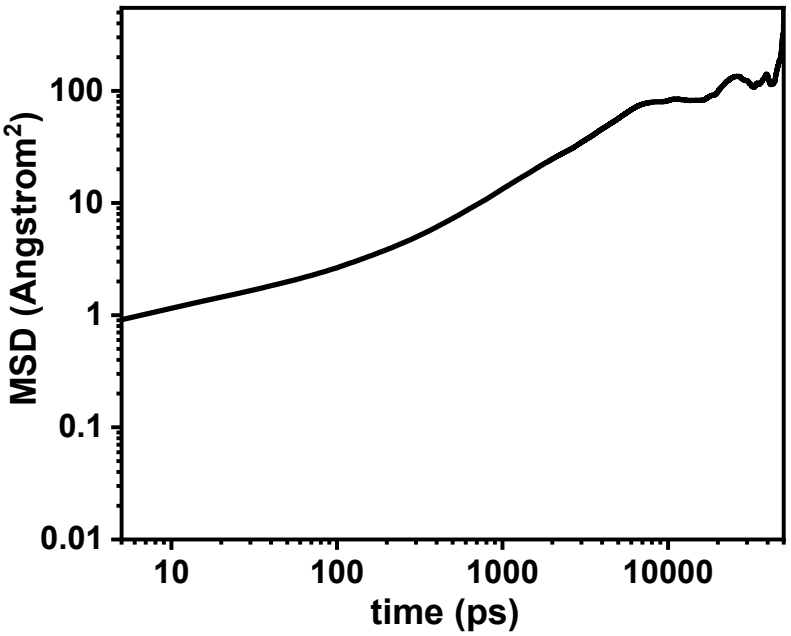

Figure S12. Tyndall effect of (a) f-sCON; (b) water and (c) f-sCON in aqueous solutions after a month.

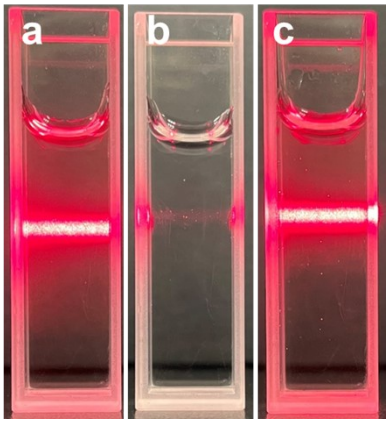

Figure S13. Size distribution of the f-sCON in aqueous solution from DLS tests.

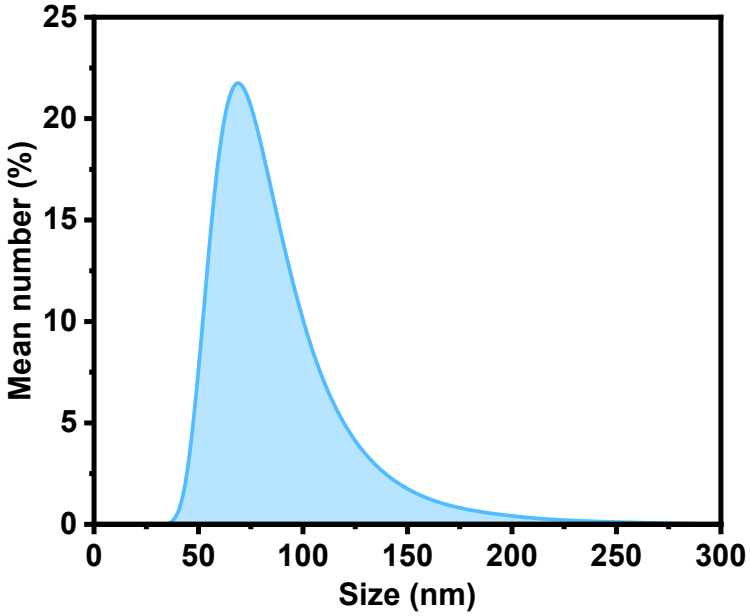

Figure S14. SEM images of (a) sulfonate-COF; and (b) f-sCON.

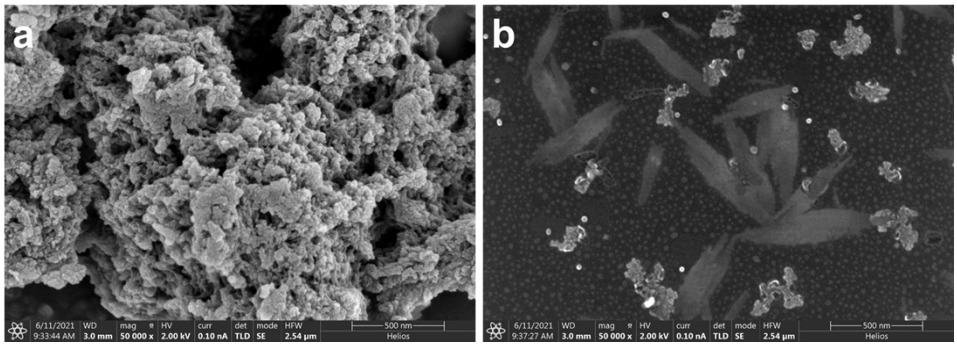

Figure S15. TEM images of sulfonate-COF.

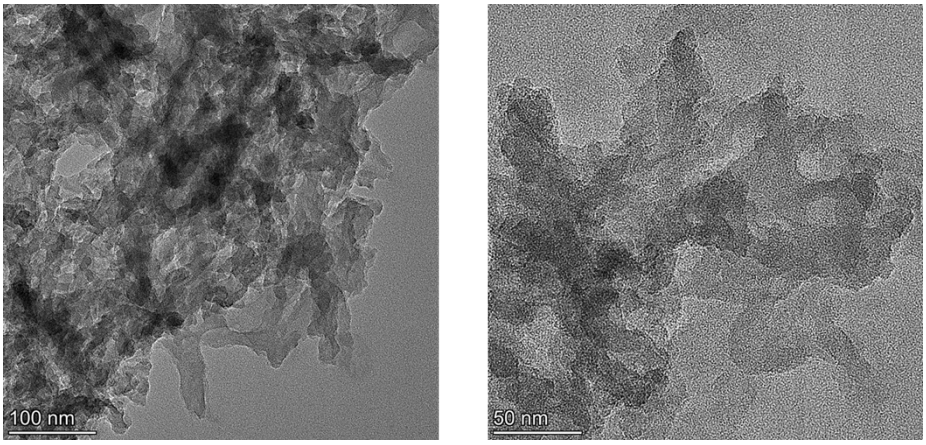

Figure S16. (a) UV–vis absorption and fluorescence spectra of f-sCON in aqueous solution.

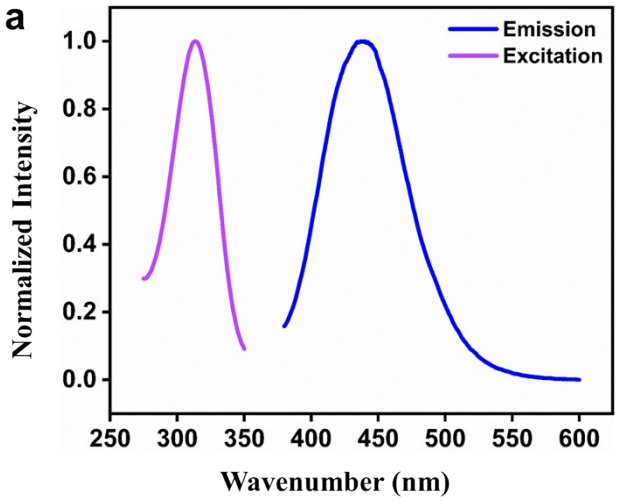

Figure S17. Solid-state fluorescence spectra of sulfonate-COF and TaPa-COF.

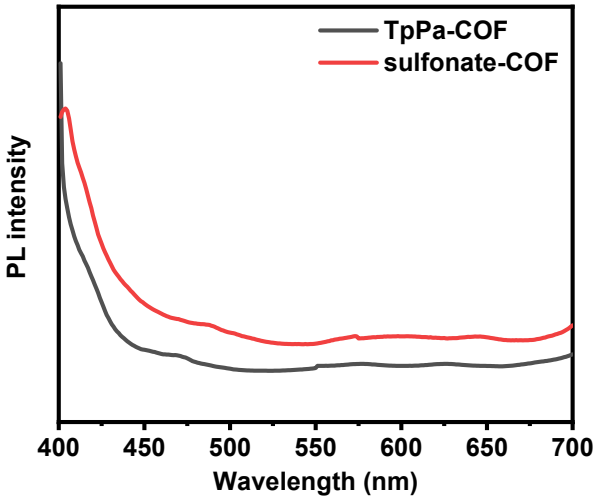

Figure S18. Electric potential of (a) DABDA and (b) sulfonate-COF backbone.

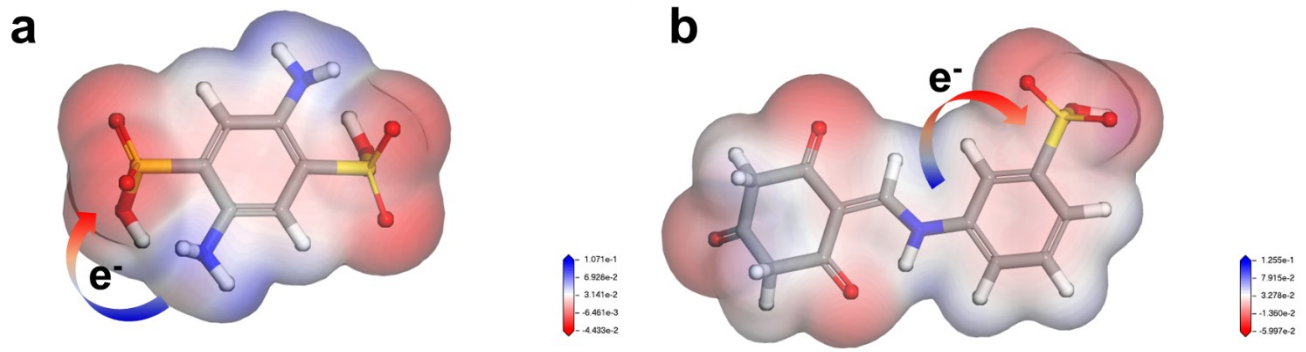

S19. Fluorescence emission spectra of f-sCON and DABDA in aqueous solution.

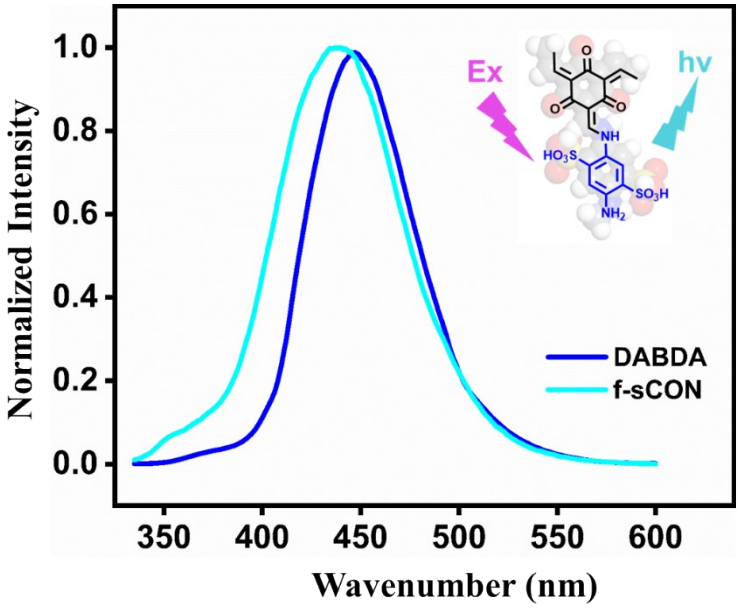

Figure S20. (a) UV–vis absorption sulfonate-COF (red) and TpPa-COF (black) in aqueous solution; (b) Fluorescence emission spectra of sulfonate-COF (red) and TpPa-COF (black) in aqueous solution.

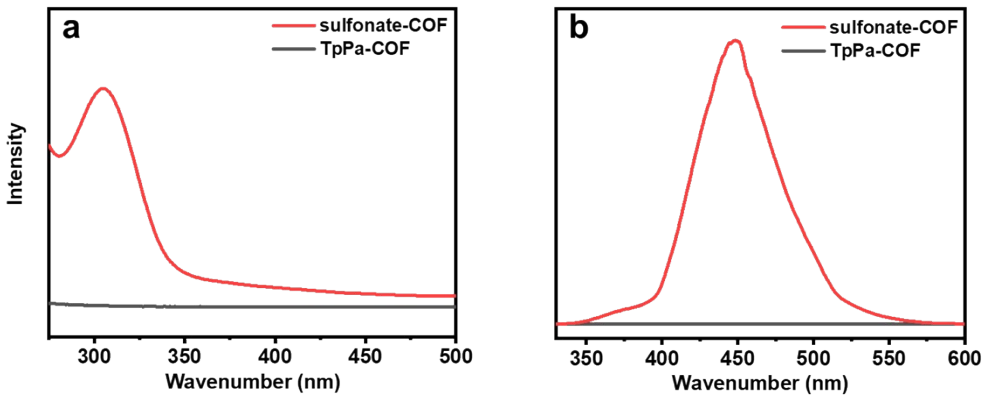

Figure S21. Fluorescence spectra of f-sCON in different solution; Inset: Fluorescent photographs of f-sCON in different solution.

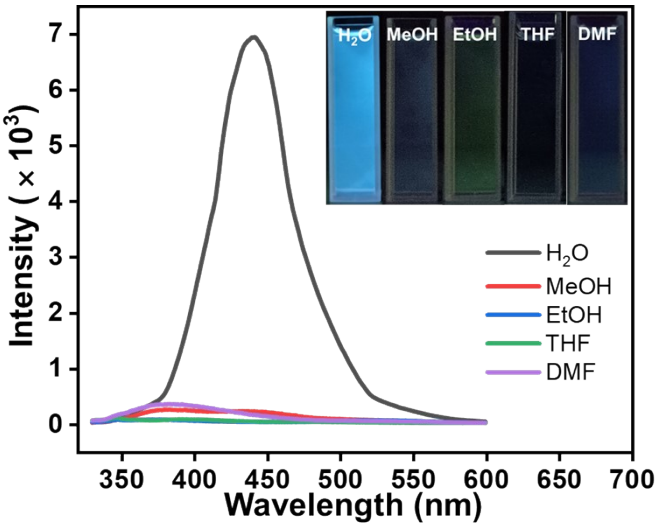

Figure S22. Binding energy of (a) sulfonate-COF-sulfonate-COF; (b) sulfonate-COF-Water; (c) sulfonate-COF-Tetrahydrofuran; (d) sulfonate-COF-Ethanol; (e) sulfonate-COF-Methanol; (f) sulfonate-COF-N,N-Dimethylformamide.

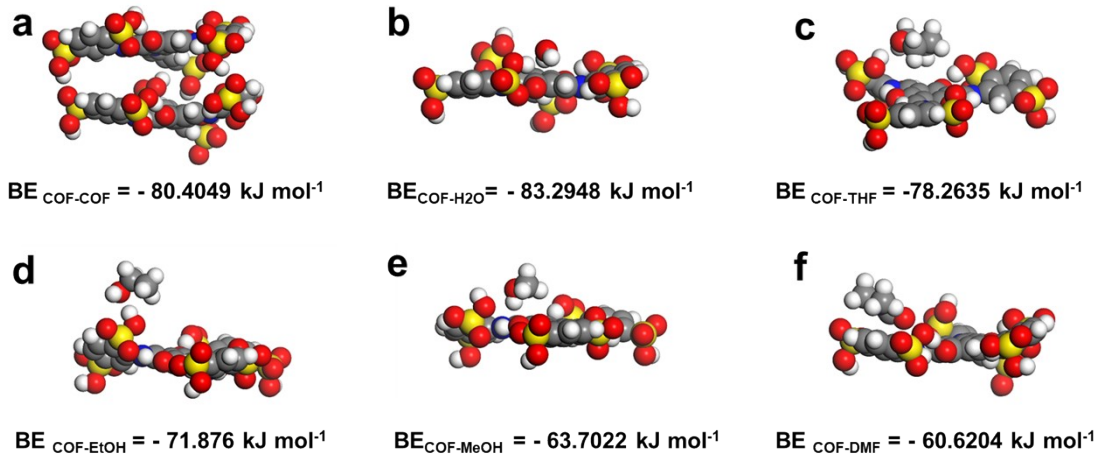

Figure S23. Effect on the emission spectra of f-sCON dispersed in water upon the incremental addition of 83 μM aqueous solution of CTC (left); Stern-Volmer plots of corresponding analyte (right).

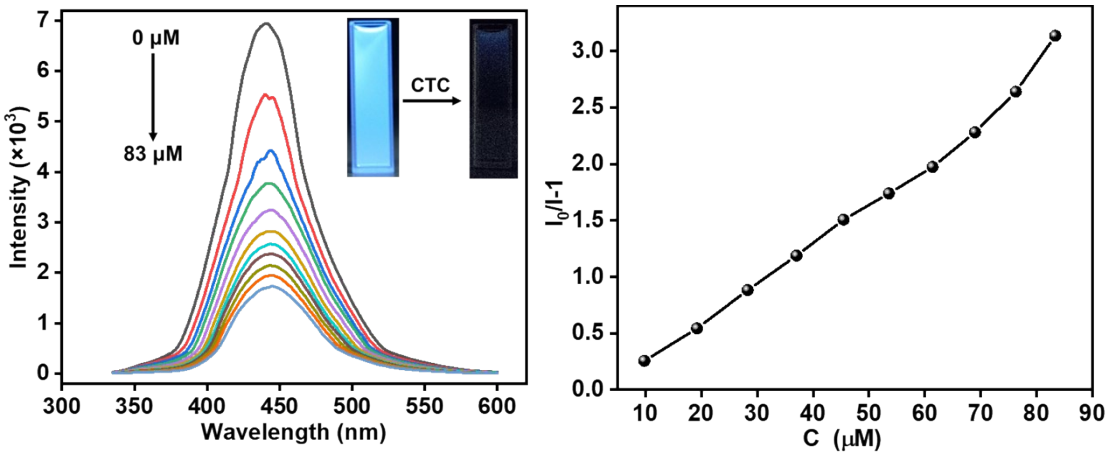

Figure S24. Effect on the emission spectra of f-sCON dispersed in water upon the incremental addition of 83 μM aqueous solution of DOX (left); Stern-Volmer plots of corresponding analyte(right).

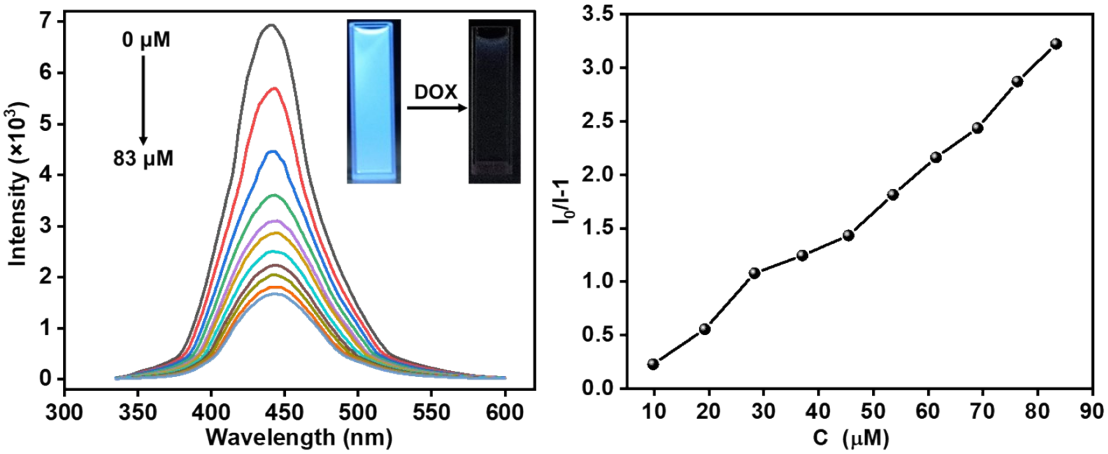

Figure S25. Effect on the emission spectra of f-sCON dispersed in water upon the incremental addition of 83 μM aqueous solution of TER (left); Stern-Volmer plots of corresponding analyte(right).

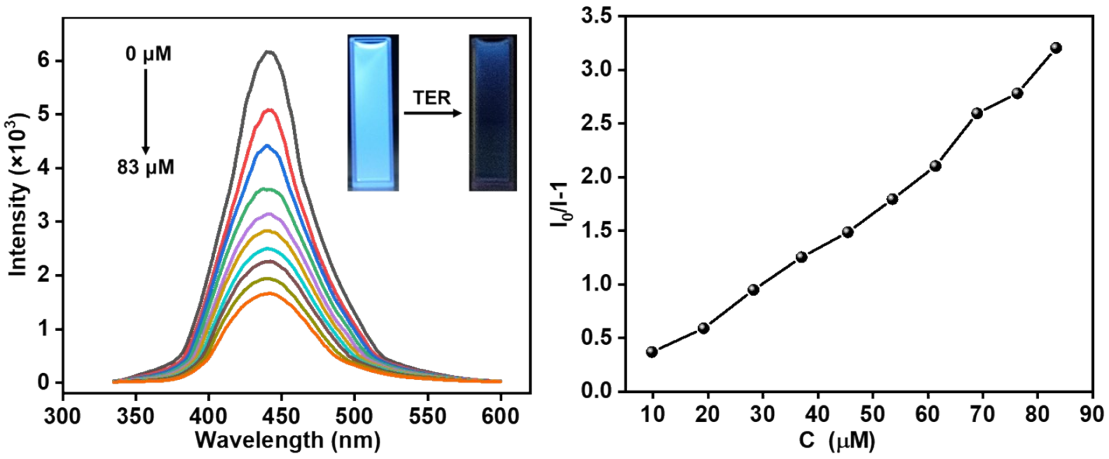

Figure S26. Effect on the emission spectra of f-sCON dispersed in water upon the incremental addition of 83 µM aqueous solution of: (a) SPA; (b) KAN; (c) APC; (d) ERY.

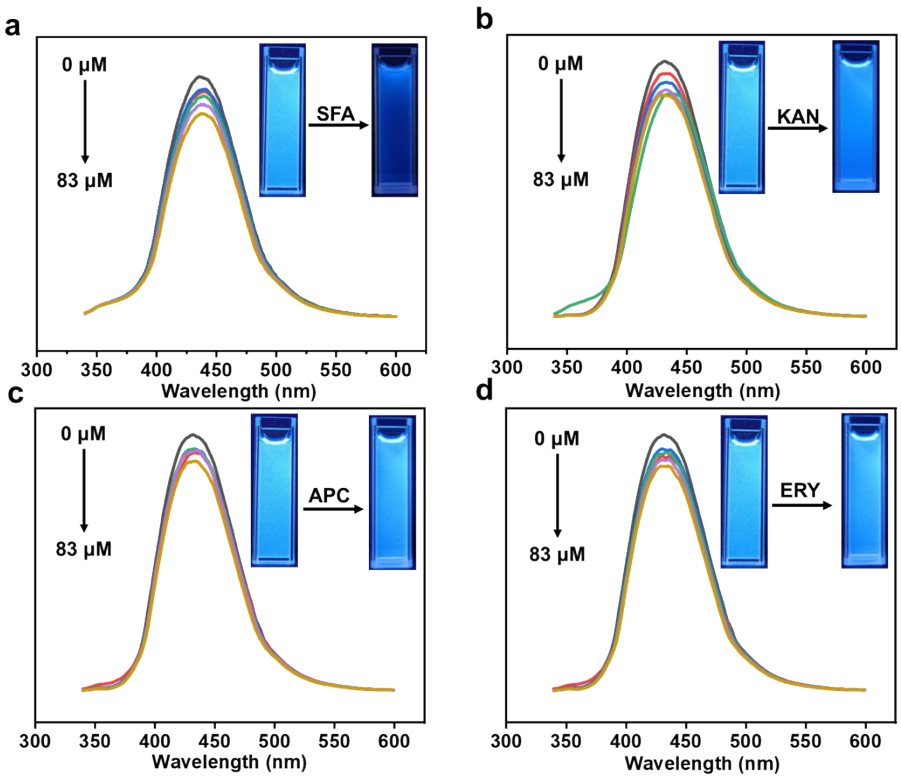

Figure S27. PXRD patterns of pristine sulfonate-COF (red) and regenerated sulfonate-COF (black).

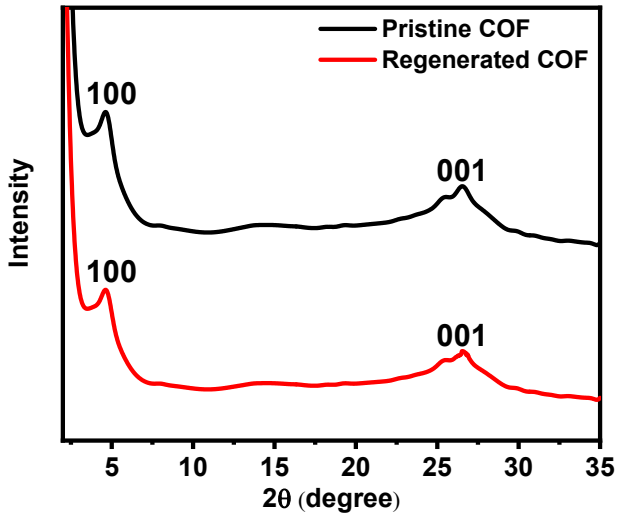

Figure S28. Adsorption isotherms and the Langmuir model fitting curves of antibiotics adsorption performance on sulfonate-COF (a) CTC; (b) DOX; (C) TER.

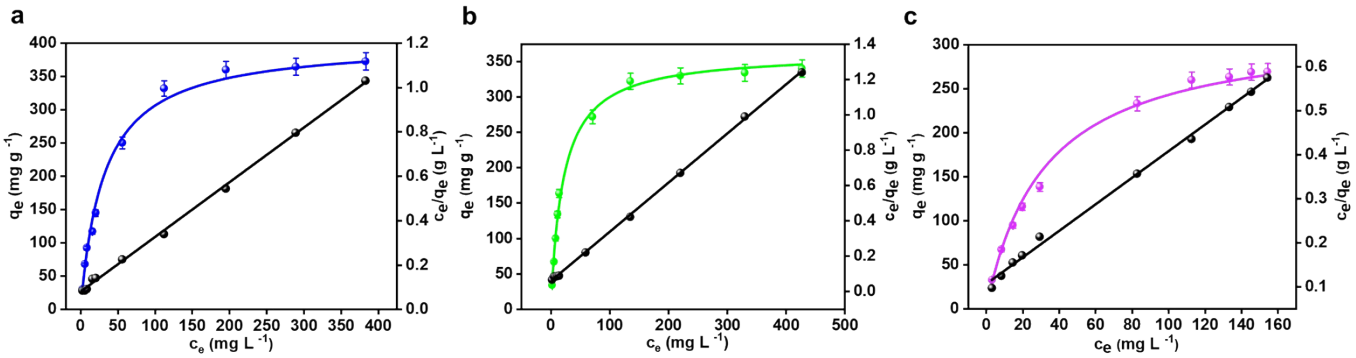

Figure S29. Adsorption kinetics curves and the pseudo-second order kinetic model fitting curvesof antibiotics adsorption performance on sulfonate-COF (a) CTC; (b) DOX; (C) TER.

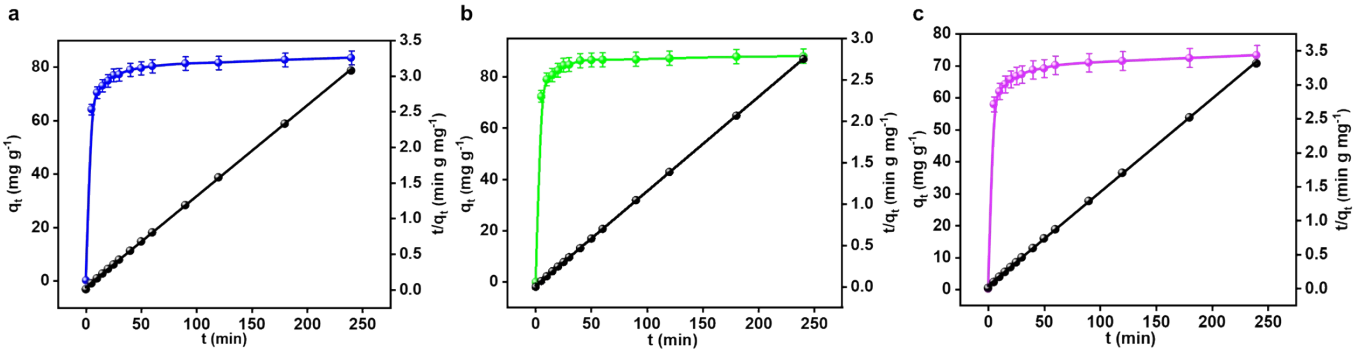

Figure S30. Schematic diagram of the experimental apparatus used for the dynamic adsorption experiment.

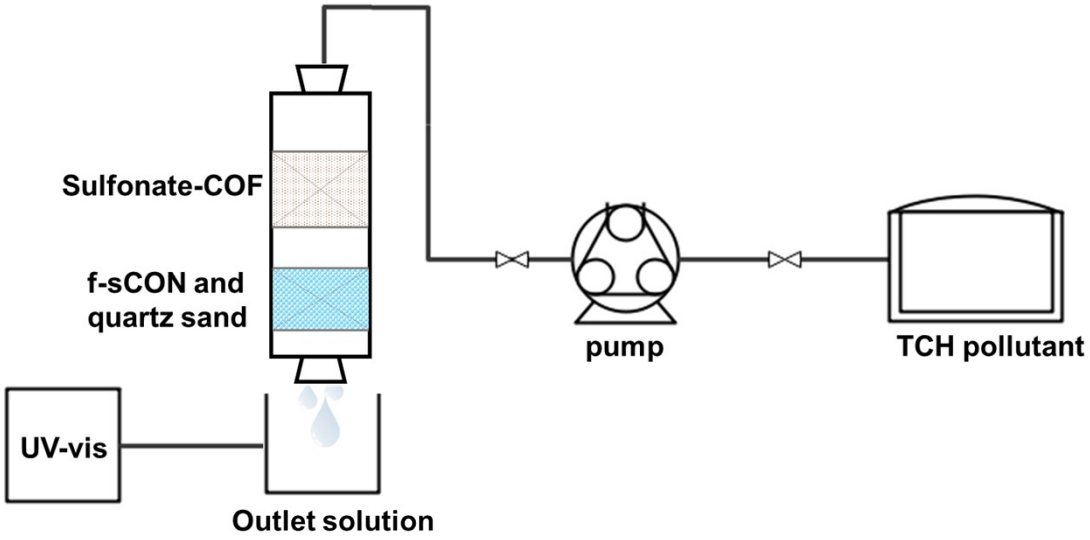

Supporting Tables

Table S1. Element contents and porosity of sulfonate-COF and TpPa-COF.

		Elemental Analysis (Wt. %)					Porous Properties	
		N	C	H	O	S	BET ($m^2 g^{-1}$)	Pore size (Å)
sulfonate-COF	Exp.	8.11	38.92	3.538	36.736	10.061	105	14
	Cal.	6.36	42.26	2.75	32.70	14.56	/	14
TpPa-COF	Exp.	11.36	62.36	4.749	19.27	/	514	17
	Cal.	9.99	68.56	4.32	17.12	/	/	18

Table S2. The detection performance of f-sCON for toward tetracycline antibiotics.

Antibiotics	K_{sv} ($10^{\wedge 4}$)	LOD (nM)	Qc (%)
TCH	4.6	48.4	82
DOX	3.9	57.8	76
CTC	3.8	56.1	75
TER	3.3	67.5	73

Table S3. The parameters of the adsorption isotherms of antibiotics on sulfonate-COF based on Langmuir and Freundlich isotherm models.

Antibiotics	Langmuir			Freundlich		
	Qm（mg g^{-1}）	K_L	R_L^2	K_F	n	R_F^2
TCH	436	0.0276	0.99424	34.4808	2.1904	0.95784
CTC	402	0.0309	0.98936	29.1548	2.1055	0.9375
DOX	362	0.0504	0.99364	39.2476	2.4832	0.88935
TER	320	0.0306	0.99173	21.0603	1.9081	0.98209

Table S4. The parameters of the adsorption kinetic of antibiotics on sulfonate-COF based on pseudo-first-order, pseudo-second-order model parameters.

Antibiotics	pesudo-second-order				pesudo-first-order		
	C_0 (mg/L)	K_2 (g min mg^{-1})	$Q_{e\ cal}$ (mg/g)	R^2	K_1 (min^{-1})	$Q_{e\ cal}$ (mg/g)	R^2
TCH	50	5.831×10^{-3}	81.77	0.99979	1.141×10^{-2}	14.5336	0.67389
CTC	50	6.126×10^{-3}	78.37	0.99987	1.686×10^{-2}	14.1723	0.81481
DOX	50	1.035×10^{-2}	87.49	0.99997	2.008×10^{-2}	9.7822	0.77525
TER	50	1.380×10^{-2}	72.57	0.99981	1.791×10^{-2}	14.3345	0.8464

Table S5. Comparison of the detection and adsorption performance for TCH with sate-of-the-art materials.

No.	Materials	LOD (nM)	Q_m (mg g^{-1})	Ref.
1	Zn-MOF	17.1	/	4
2	Ag(0)@Ag(I)–SR	470	/	5
3	UiO-66-NH2@TpTt-COF	7.4	/	6
4	IPQDs@MIPs	28	/	7
5	LMOF	110	/	8
6	SN-SiNPs	9.5	/	9
7	AG-ZIF	/	456.62	10
8	101(Fe)	/	420.6	11
9	CSMan-gCNMZnO0.3	/	164.63	12
10	MCCSATiO2	/	152.89	13
11	C–ZnO0.5/ZAA	/	418.81	14
12	1-HBPP	/	697.6	15
13	CMP-LS8	220.4	909.09	16
14	Uio67/NSC	131.3	427.35	17
15	PFPT	14.2	3.12	18
16	PCN-128Y	30.1	423	19
17	**sulfonate-COF**	**48.4**	**436**	**This work**

References

[S1] J. H. Chong, M. Sauer, B. O. Patrick, M. J. MacLachlan, Org. Lett. **2003**, 5, 3823-3826
[S2] J. Xu, S. H. An, X. Y. Song, Y. J. Cao, N. Wang, X. Qiu, Y. Zhang, J. W. Chen, X. L. Duan, J. H. Huang, W. Li, Y. G. Wang, Adv. Mater. **2021**, 2105178.
[S3] Y. Z. Tang, H. L. Huang, W. J. Xue, Y. J. Chang, Y. Li, X. Y. Guo, C. L. Zhong, Chem. Eng. J. **2020**, 384, 123382
[S4] J. Chen, F. H. Xu, Q. Zhang, S.Y. Li, X. Q. Lu, Analyst. **2021**, 146, 6883-6892
[S5] Y. Zhang, M. Lv, P. F. Gao, G. M. Zhang, L. H. Shi, M. J. Yuan, S. M. Shuang, Sens Actuators: B. **2021**, 326, 129009
[S6] C. H. Li, X. Xu, J. Y. Xing, F. L. Wang, Y. B. Shi, X. Zhao, J. Liu, Y. Yang, Z. L. Zhao, Appl. Surf. Sci. **2023**, 616, 156455
[S7] X. Wei, S. Zhang, T. Wang, A. X. Chen, J. F. Guo, B. Bai, S. K. Yang, Y. Q. Li, X. Y. Wang, X. N. Liu, J. Mater. Chem. C, **2022**, 10, 8432-8440
[S8] C. Yazhini, J. Rafi, P. Chakraborty, S. Kapse, R. Thapa, B. Neppolian, J. Clean. Prod. **2022**, 373, 133929
[S9] Y. F. Wang, Z. Li, M. Jiang, X. Yu, L. Xu, Sci. Total. Environ. **2022**, 846, 157470
[S10] Y. Kong, Y. Zhuang, K. Han, B. Y. Shi, Colloids and Surfaces A. **2020**, 588, 124360
[S11] Z. Zhang, Y. Chen, Z. Wang, C. Y. Hu, D. C. Ma, W. Q. Chen, T. Q. Ao, Applied Surface Science. **2021**, 542, 148662
[S12] Z. H. Li, H. B. Li, X. L. Zeng, S. M. Liu, Y. S. Yang, Chem. Eng. J. **2023**, 458, 141455
[S13] C. J. Xiao, Y. K. Yan, G. D. Wen, Y. T. Zhou, D. Na, C. L. Yang, J. S. Zhang, Materials & Design, **2023**, 226, 111620
[S14] T. J. Ji, H. Z. Zhang, S. J. Shah, Y. C. Wang,W. X. Gong, . M. Wang, L. Pan, H. B. Ji, G. N. Chen, Z. X. Zhao, Z. X. Zhao, J. Mater. Chem. A, **2022**, 10, 22571-22583
[S15] Y. L. Liu, H. Y. Zhou, X. Zhou, C. Jin, G. F. Liu, S. P. Huo, F. X. Chu, Z. W. Kong, Chemosphere, **2023**, 316, 137798
[S16] S. Wang, Q. B. Hu, Y. C. Liu, X. Y. Meng, Y. Ye, X. H. Liu, X. W. Song, Z. Q. Liang, J. Hazard. Mater. **2020**, 387, 121949
[S17] Q. F. Yang, Q. Hong, Y. K. Luo, Chem. Eng. J. **2020**, 392, 123680
[S18] A. H. Malik, P. K. Iyer, ACS Appl. Mater. Interfaces. **2017**, 9, 4433-4439
[S19] Y. Zhou, Q. Yang, D. N. Zhang, N. Gan, Q. P. Li, J. Cuan, Sens. Actuators, B. **2018**, 262, 137-143